Scalable In-Fiber Manufacture of FunctionalComposite Particles

Minghui Du,[†,¶] Shubiao Ye,[‡] Junzhou Tang,[†,¶] Shichao Lv,[†,¶] Jiejie Chen,[†,¶] Jiri Orava,[§] Guangming Tao,[∥] Ping Lan,[‡] Jianhua Hao,[⊥] Zhongmin Yang,[†,¶] Jianrong Qiu,[#]
and Shifeng Zhou*[,†,¶]

[†]State Key Laboratory of Luminescent Materials and Devices, School of Materials Science and Engineering, South China University of Technology, Guangzhou 510640, China

[¶]Guangdong Provincial Key Laboratory of Fiber Laser Materials and Applied Techniques, Guangdong Engineering Technology Research and Development Center of Special Optical Fiber Materials and Devices, Guangzhou 510640, China

[‡]Guangdong Provincial Key Laboratory of Colorectal and Pelvic Floor Diseases, The Sixth Affiliated Hospital of Sun Yat-Sen University, Guangzhou 510655, China

[§]IFW Dresden, Institute for Complex Materials, Helmholtzstr. 20, Dresden 010 69, Germany

[∥]School of Optical and Electronic Information, Wuhan National Laboratory for Optoelectronics, Huazhong University of Science

and Technology, Wuhan 430074, China

[⊥]Department of Applied Physics, The Hong Kong Polytechnic University, Hung Hom, Kowloon, Hong Kong China

[#]State Key Laboratory of Modern Optical Instrumentation, School of Materials Science and Engineering, Zhejiang University, Hangzhou 310027, China

ABSTRACT: Advanced fabrication methods must be developed for magnetic−polymeric particles, which are used in medical diagnostics, drug delivery, separation, and environmental remediation. The development of scalable fabrication processes that enables simultaneously tuning of diameters and compositions of magnetic−polymeric particles remains a major challenge. Here, we proposed the production of high-quality magnetic-composite particles through a universal method based on the in-fiber Plateau−Rayleigh instability of polymeric fibers. This method can simultaneously control the particle diameter, hybrid configuration, and functional properties. The diameter of magnetic−polymeric particles can be reproducibly tuned from ∼20 nm to 1.25 mm, a wide range unachievable by conventional solution methods. The final diameter was controlled by the inner/outer fiber diameter ratio. We further showed that the prepared magnetic−polymeric composite particles can be used for the highly efficient recovery of heavy metals (98.2% for Cd2+) and for the precise separation of immune cells (CD4+ T cells). Overall, the in-fiber manufacture method can become a universal technology for the scalable preparation of different types of magnetic−polymeric composite particles with diverse functionalities.

KEYWORDS: fibers, magnetic−polymeric particles, fluid dynamical instability, heavy-metal recovery, cell separation

Introduction

The application of magnetic−polymeric particles has revolutionized various fields, such as magnetic resonance imaging,[1] drug delivery,[2] chemical sensing,[3] environmental remediation,[4] optical sensing,[5] and energy harvesting.[6,7] Future applications of composite particles are mainly driven by advancements in synthesis methodologies. Conventional chemical approaches have limited capabilities to tune the particle diameter and structure, and they must satisfy stringent limits over a set of experimental variables, such as concentration, dosage, and the nature of solvents and precursors, all of which must be controlled to attain the desired properties.[8−12] Additionally, chemical routes are hampered by unexpected coalescence and agglomeration during particle growth, and the obtained products are typically characterized by a broad particle size distribution. Although microfluidic or templated methods may partially overcome these issues, these techniques mainly rely on prefabricated structures and devices.[13−17] Additionally, both types of methods are strictly limited to a specific combination of materials and particle sizes that can be used/obtained and are particularly suited for low-viscous and small-sized polymeric candidates. Despite the recent progress in magnetic−polymeric particle synthesis,[18−20] developing a scalable fabrication method that can continuously tune the particle diameter from nanometer- to

micrometer-scales remains a challenge. Here, we described a methodology for the scalable synthesis of magnetic–polymeric particles that exploits in-fiber fluid dynamical instabilities. The in-fiber manufacture method was originally tested for the fabrication of photonic[21] and polymeric nanoparticles.[22] We proposed an effective method for producing composite particles with interesting magnetic and photoluminescence (PL) properties. This technique can realize the rapid preparation of various polymeric-derived magnetic particles and tune the particle diameter over an exceptionally wide range of ~20 nm to ~1.25 mm. We demonstrated the application of magnetic–polymeric particles for efficient cell separation.

RESULTS AND DISCUSSION

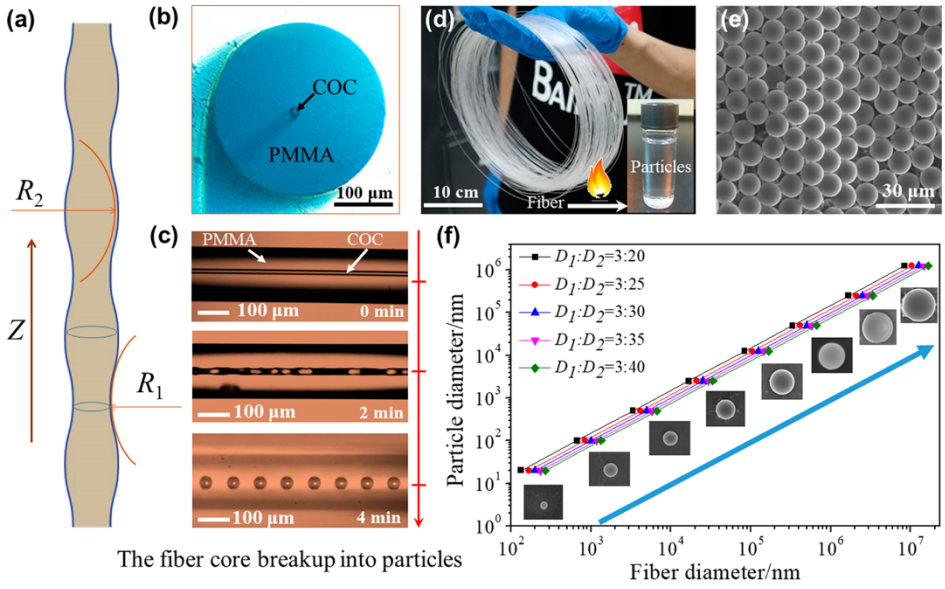

Figure 1. Particles fabricated by in-fiber PRI method. (a) The PRI phenomenon of an intermediate stage of a jet breaking up into droplets. (b) The cross section of the COC-PMMA fiber. (c) The fiber at different annealing times ranging from 0 to 4 min. (d) A bundle of fibers and the obtained particles in DMAC solution. (e) SEM image of the synthesized COC particles. (f) The linear-scaling relation between the resultant fiber and the particle diameter.

The fabrication method was inspired by the Plateau–Rayleigh instability (PRI) phenomenon.[23,24] As illustrated in Figure 1, a perfectly cylindrical viscous stream is highly likely to spontaneously form droplets upon the application of an external perturbation. The process is dominated by the surface tension γ and can be described by the Young–Laplace equation as follows:[25,26]

$$\Delta P = \gamma\left(\frac{1}{R_1} + \frac{1}{R_2}\right)$$

where ΔP is the pressure difference across the fluid interface, and R_1 and R_2 are the principal curvature radii. The Young– Laplace equation shows that the pressure was higher in the pinched sections (lower in the bulged sections) of a jet and that the existing pressure gradient induced the flow. This internal flux resulted in a displacement amplitude and a greater surface tension, which ultimately formed a droplet through the rupture of the pinched points. The bulged areas naturally formed spherical droplets because of surface-energy mini- mization. The diameter of the formed spherical droplet was determined by two factors: the perturbations rate and the wavelength at which instabilities grew. The relation among the rate of perturbations τ, the core (cylindrical fluid) diameter D_0, and the instability wavelength λ can be described by the Tomotika's linear stability theory as follows:[27,28]

$$\tau = D_0\mu_{\text{clad}}/[\gamma_{\text{i}}(1 - \eta^2)\Phi(\eta, \mu_{\text{core}}/\mu_{\text{clad}})]$$

where μ_{core} and μ_{clad} are the viscosities of two materials in contact, and μ_{clad} can typically be air for a one-material jet, for example, water. The interfacial surface tension between the two materials is represented by γ_{i}. The dimensionless constant η depends on the relative viscosities of the core and the cladding materials, and Φ is a defined function.[29] The instability wavelength λ can be expressed in terms of the core diameter as $\lambda = \pi D_0/\eta$. Under the assumption of an incompressible flow of the core viscous material, the final droplet diameter D can be tuned by controlling the initial core diameter D_0 as follows:

$$D = \sqrt[3]{3\pi/2\eta}\, D_0$$

To validate the aforementioned relations, an in-fiber PRI approach was adopted because of its capability to maintain an extremely uniform and stable cylindrical viscous stream, which is crucial for inducing a stable PRI evolution, shown in Figure 1a. Cyclic olefin copolymer (COC) was selected as the prototype material for the fiber core because it has excellent thermal stability, which is beneficial in the nanoparticle formation stage.[30,31] A typical fabrication was performed in three steps: (1) A COC preform was inserted into a protective poly(methyl methacrylate) (PMMA) tube, and a fiber was drawn at a speed of 0.3 m s^{-1} at 255 °C until the required core diameter D_0 was reached. Figure 1b shows a representative optical micrograph of the fabricated COC-PMMA fiber cross section with D_0 = 12.5 μm. (2) The COC-PMMA fiber was heated at 265 °C for 4 min to trigger the particle formation. The optical transmission micrographs (Figure 1c) revealed the typical

stages of particle formation. The intact cylindrical core (0 min of annealing) transformed into a sinusoidal core after 2 min of annealing, until the unstable core was broken up to spherical particles (4 min). (3) Highly uniform COC particles (scanning electron microscopy (SEM), Figure 1e) with a diameter of ~12.8 ± 0.5 μm, were obtained by dissolving the outer core PMMA in N,N-dimethylacetamide (DMAC) solution (Figure 1d,e). The schematics of the fiber-drawing process and the breaking up process of the fiber core into particles are presented in Figure S1 in the Supporting Information. The key advantage of PRI method is that it can produce particles with highly uniform sizes and high yields. In principle, 1.5×10^7 particles with a final diameter of 100 nm can be obtained using a single fiber that is 1 m long and 1 mm in diameter. The particle yield can be multiplied using a stack- and-draw process in a multicore fiber.

Once the fiber-drawing process can be controlled, we investigated the effects of the initial fiber configuration and conditions during the fiber-drawing process on the structure and size of the prepared particles. Five groups of PMMA fiber preforms were designed with PMMA fiber that had a constant inner diameter (D_1 = 3 mm) and different outer diameters (D_2 = 20, 25, 30, 35, and 40 mm). The resultant fibers with varying outer diameters were tested after the drawing. The diameter of the fabricated particles scaled linearly with the outer diameter of the resultant fiber, and the particle diameter was precisely controlled from 20 nm, 100 nm, 500 nm, 2.5 μm, 12.5 μm, 50 μm, and 250 μm to 1.25 mm by adjusting the outer diameter of the resultant fiber from 0.3, 1.3, 6.7, 33.3, 167, and 667 to 16663 μm (Figure 1f, micrographs). This outstanding tunability of the particle size over 4 orders of magnitude in diameter was difficult to achieve by conventional solution- based methods. Additionally, the particle size can be tuned by changing the inner (D_1) and outer diameters of the preform (D_2), as shown in Figure 1f.

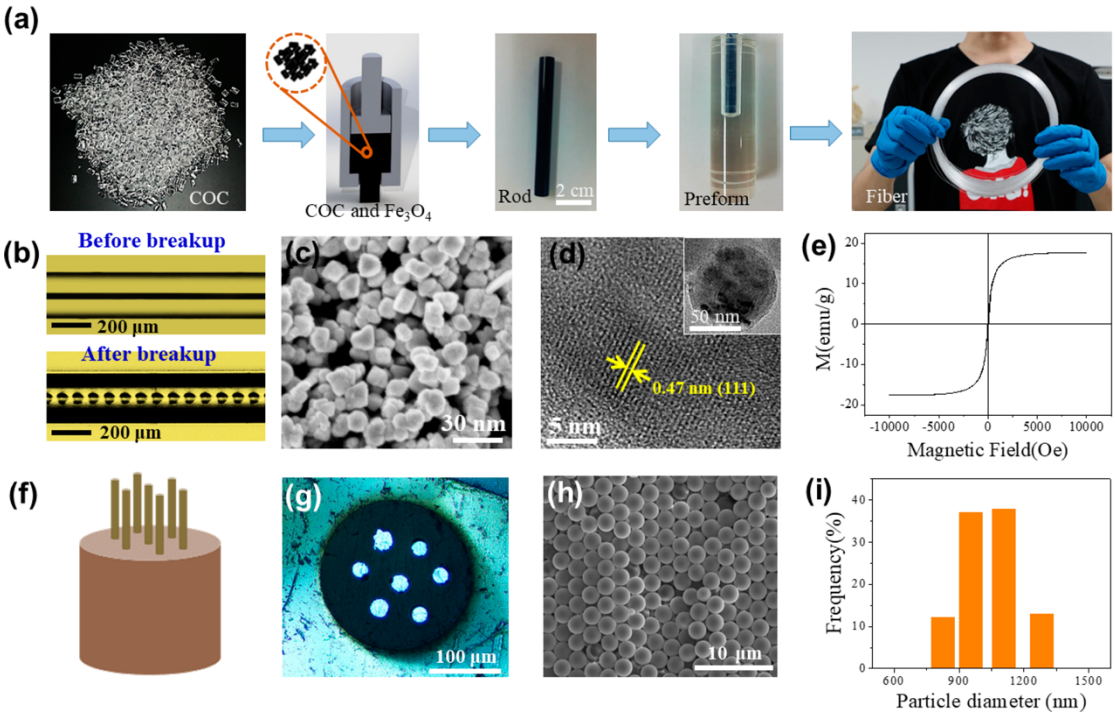

Figure 2. Magnetic–polymeric particles fabricated by in-fiber PRI method. (a) Schematic of the preparation procedure of fiber. (b) The magnetic fiber core breaking up into particles. (c) SEM image of the raw Fe_3O_4 nanoparticles. (d) High-resolution TEM image of the polymer-composite particles. The inset shows a single particle. (e) VSM hysteresis loop of the particles. (f, g) The preform with seven cores. (h, i) SEM image of the particles and their size distribution.

To further test the in-fiber PRI approach, we synthesized magnetic composite particles, such as magnetic–polymeric particles, by controlling the design, structure, and constituents of the fibers. The detailed fabrication process of the magnetic– polymeric particles is depicted in Figure 2. Composite rods consisting of a mixture of 90 wt % of COC pellets and 10 wt % of Fe_3O_4 nanoparticles were fabricated by melt compounding and extrusion using a custom-built extrusion machine (Figure 2a). The rod was inserted into a PMMA tube, which was then consolidated under vacuum, and the preform structure was formed. A composite fiber was thermally drawn by a fiber-drawing tower specifically designed for the PRI experiments. As expected, thermal treatment of the fiber induced a PRI phenomenon, which resulted in the formation of orderly arranged spherical particles because of the continuous breaking of the magnetic core (Figure 2b). The magnetic–polymeric particles can subsequently be released by dissolving the PMMA cladding in DMAC solution. The Fe_3O_4 nanoparticles before (Figure 2c) and after (Figure 2d) their incorporation into the polymeric particle matrix were characterized by SEM and transmission electron microscopy (TEM). As shown in Figure 2c,d, the average diameter of the nano-Fe_3O_4 particles was ∼10–20 nm, and the particles maintained their initial morphology without a noticeable degradation during the fiber drawing. The SEM image and the diameter distribution of the particles made from a single core fiber are presented in Figure S2 in the Supporting Information. The high-resolution TEM (Figure 2d) and TEM images (the inset in Figure 2d) of the released magnetic–polymeric particles displayed that the nano-Fe_3O_4 particles were homogeneously dispersed inside the COC particles.

The magnetic properties of the polymer COC nano-Fe_3O_4 composite particles were examined. The vibrating sample magnetometer (VSM) measurement (Figure 2e) revealed that the magnetic behavior of the composite particles was approximately linear without significant hysteresis because of the negligible coercive field ($H_c \approx 5$ Oe). In subsequent experiments, the operating magnetic field was in the range of several kOe. The magnetic induction intensity of the fabricated particles was estimated as ∼18 emu g^{-1}, which confirmed their promising application in a rapid magnetic separation when an external magnetic field is applied.

Additionally, we introduced nano-Fe_3O_4 particles into several types of polymers, such as acrylonitrile butadiene styrene (ABS), cyclic olefin polymer (COP), and polycar- bonate (PC) to

demonstrate the universality of the in-fiber PRI approach for magnetic–polymeric particle fabrications. To date, these magnetic–polymeric particles have not been reported elsewhere despite their intriguing biochemical, mechanical, and optical properties (Table S1 in the Supporting Information). These polymers are nontoxic and have a good biocompatibility. Additionally, these materials display excellent optical properties and are highly transparent in the visible spectral range. The synthesized composite particles can potentially exhibit high-intensity luminescence by incorporat- ing various optically active centers, as will be subsequently demonstrated in this paper. Moreover, these polymers exhibit excellent mechanical and thermoplastic properties, which allow for the successful and scalable fabrication of composite particles on the basis of the in-fiber PRI.

The in-fiber PRI approach can also be used for multicore fibers to realize the scalable synthesis of magnetic–polymeric particles. For example, a preform containing seven cores was fabricated by inserting seven identical COC-Fe_3O_4 composite rods into a PMMA tube. Then, the preform was thermally drawn into fibers (Figure 2f). Figure 2g presents the optical transmission micrograph of the cross section of the fiber containing seven magnetic cores. Thermal treatment of the fiber at 265 °C led to the simultaneous breaking up of all cores into a 3D particle arrangement. The SEM image showed that the obtained magnetic–polymeric particles were nearly monodispersed and had a uniform diameter in COC (Figure 2h). Dynamic light scattering (DLS) measurement confirmed the very narrow particle size distribution with an average diameter of ∼1.1 ± 0.1 μm (Figure 2i). To study the relation between the fiber-drawing conditions and the composite particle yield, we tested different fiber-drawing speeds. As an example, a fiber with a diameter of ∼200 μm and a fiber- drawing speed of ∼0.3 m s^{-1} was evaluated. The yield of the composite particles (diameter: ∼100 nm) was ∼8 × 10^9 particles per hour. Then, the fiber-drawing speed was increased to ∼0.5 m s^{-1} for the same fiber. Consequently, the yield of the composite particles (diameter: ∼100 nm) became ∼1.35 × 10^{10} particles per hour. These results proved that the production yield was mainly limited by the fiber configuration and the fiber-drawing speed, and that the method has a great potential for nanoparticle fabrication when all parameters are optimized.

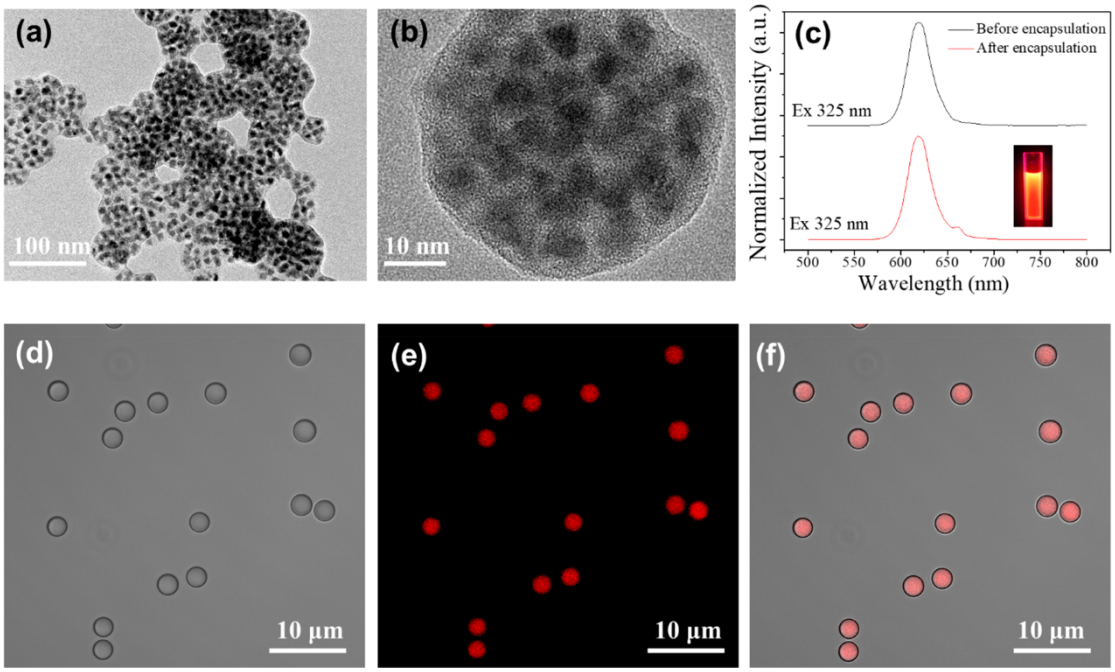

Figure 3. PL composite particles prepared by in-fiber PRI approach. (a) TEM image of the CdSe/ZnS QDs inside the polymeric particle. (b) HRTEM image of a single polymeric particle. (c) PL characterization of the QDs before and after the encapsulation. (d–f) Bright-field, fluorescence, and overlay images of the particles embedded with rhodamine.

The in-fiber PRI approach also enabled the additional functionalization of magnetic–polymeric particles by modifying the precursors. For example, by incorporating quantum dots (QDs) or organic dyes into a precursor biocompatible polymeric rod, the particles gained intriguing optical properties (Figure 3). The TEM images (Figure 3a,b) showed that dense CdSe/ZnS QDs were homogeneously dispersed in the COC matrix. The diameter of the fabricated particles was estimated to be ~50–70 nm (Figure 3a,b). PL characterization (Figure 3c) confirmed that the fingerprint radiative electronic transitions of CdSe/ZnS QDs were well maintained in the polymeric matrix. Moreover, the characteristic shape and peak position of the CdSe/ZnS QD PL spectrum were similar to each other before and after the encapsulation, indicating that the fabrication process exerted a negligible influence on the optical properties of QDs. The inset of Figure 3c shows the PL image of the composite particles dispersed in DMAC solution under 365 nm irradiation. The size of QDs was unchanged, as confirmed by the TEM characterizations (Figures S3 and 3b). The confocal fluorescence microscopy images displayed that the luminescent dyes were well encapsulated in the polymeric particles by the in-fiber PRI approach (Figure 3d–f).

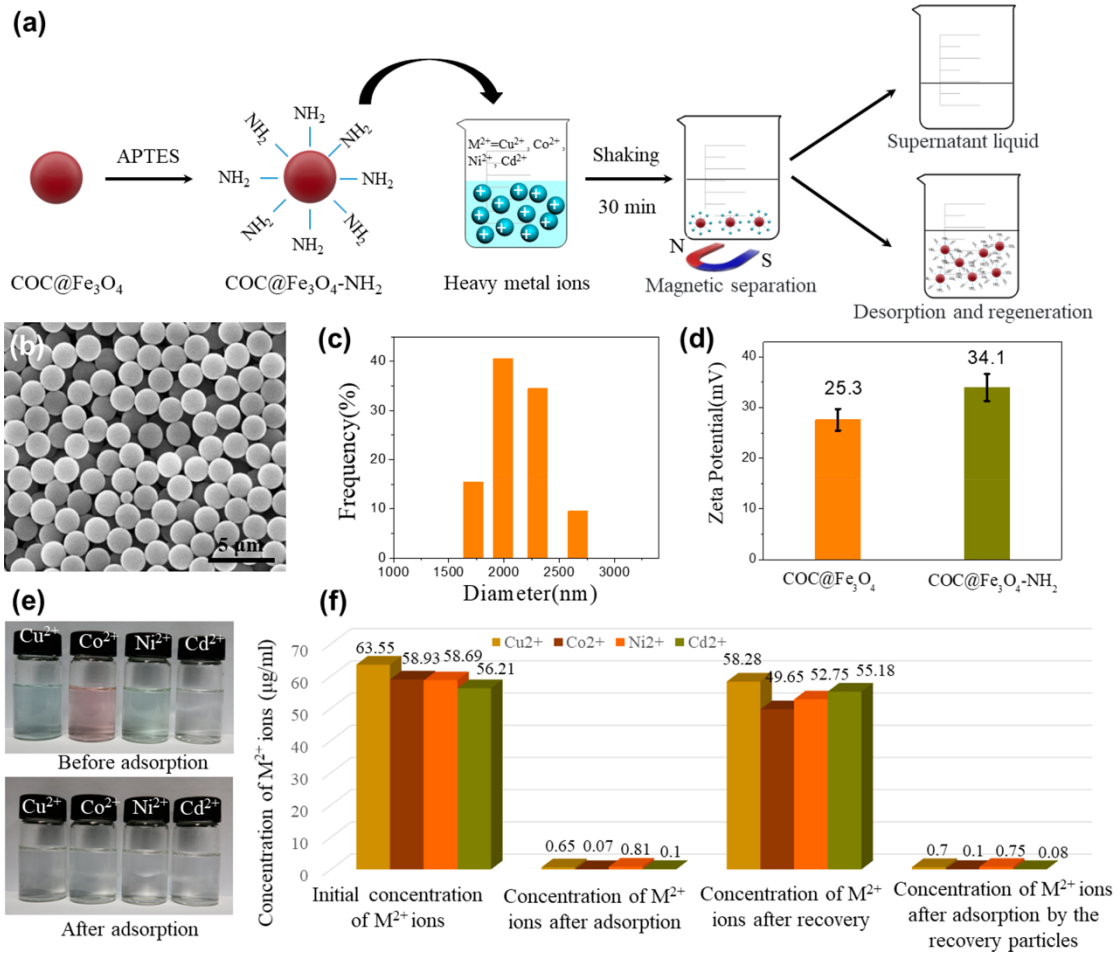

Figure 4. Heavy-metal ion recovery applications. (a) Schematic of the heavy-metal ion recovery process. (b, c) SEM image and size distribution of the particles, respectively. (d) The ζ potential of the particles before and after the functionalization. (e) Photographs comparing the solutions before and after the adsorption experiment. (f) The heavy-metal adsorption efficiency and the recovery reproducibility test.

The successful fabrication of the magnetic–polymeric particles with a controllable size motivated us to explore the separation properties composite particles in environmental remediation and cellular immunology applications. For example, by functionalizing the magnetic–polymeric particles and immobilizing amino groups on their surface, heavy-metal ions can be selectively captured by exploiting the complexation interaction between the amino groups and the heavy-metal ions.[32−35] The schematic of a heavy-metal ion separation process involving amino-modified magnetic–polymeric particles (COC@Fe_3O_4-NH_2) is shown in Figure 4a. To balance the separation capacity and the recyclability ability, the optimal diameter of the magnetic–polymeric particles was set to ~2 μm by controlling the fiber diameter (Figure 1f). The SEM image shows the uniform size distribution of the synthesized COC@Fe_3O_4-NH_2 particles (Figure 4b) with an average diameter of ~2.2 ± 0.1 μm according to DLS measurements (Figure 4c), which agreed with the prediction shown in Figure 1f. The ζ potential measurements indicated that surface modification markedly increased the ζ potential from 25.3 mV to 34.1 mV,

demonstrating the successful anchoring of amino groups on the magnetic–polymeric particles surface (Figure 4d).

In a typical separation test, the functionalized magnetic– polymeric particles were added to solutions containing Cu^{2+}, Co^{2+}, Ni^{2+}, and Cd^{2+} ions with initial concentrations of 65.35, 58.93, 58.69, and 56.21 μg mL^{-1}, respectively. The solutions immediately became colorless when brought into a contact with a magnet because of the selective uptake of heavy-metal ions (Figure 4e). Inductively coupled plasma atomic emission spectrometry (ICP-AES) analysis revealed that the concentrations of Cu^{2+}, Co^{2+}, Ni^{2+}, and Cd^{2+} ions in the solution were reduced from their initial concentrations to 0.65, 0.07, 0.81, and 0.10 μg mL^{-1}, all of which were well below the heavy- metal ions emission standards prescribed by the World Health Organization (WHO) and the United States Environmental Protection Agency (US EPA).[36,37] The energy-dispersive X-ray spectroscopy (EDX) characterizations demonstrated that Cu^{2+}, Co^{2+}, Ni^{2+}, and Cd^{2+} were successfully adsorbed by the amino- modified magnetic–polymeric particles (Figure S3 in the Supporting Information). The adsorbed heavy-metal ions were re-released in the solution, and the desorbed concentrations of Cu^{2+}, Co^{2+}, Ni^{2+}, and Cd^{2+} were measured as 58.28, 49.65, 52.75, and 55.18 μg mL^{-1}, respectively. The recycling efficiencies of Cu^{2+}, Co^{2+}, Ni^{2+}, and Cd^{2+} ions were calculated to be 89.2%, 84.3%, 89.9%, and 98.2%, respectively. Moreover, the functionalized magnetic–polymeric particles were regenerated after each use by ultrasonic washing with 0.1 mol L^{-1} NaOH solution. Only a small decrease in the separation efficiency was observed after the cycled reuse (Figure 4f). These properties make the prepared magnetic–polymeric particles ideal candidates as recyclable heavy-metal adsorbents.

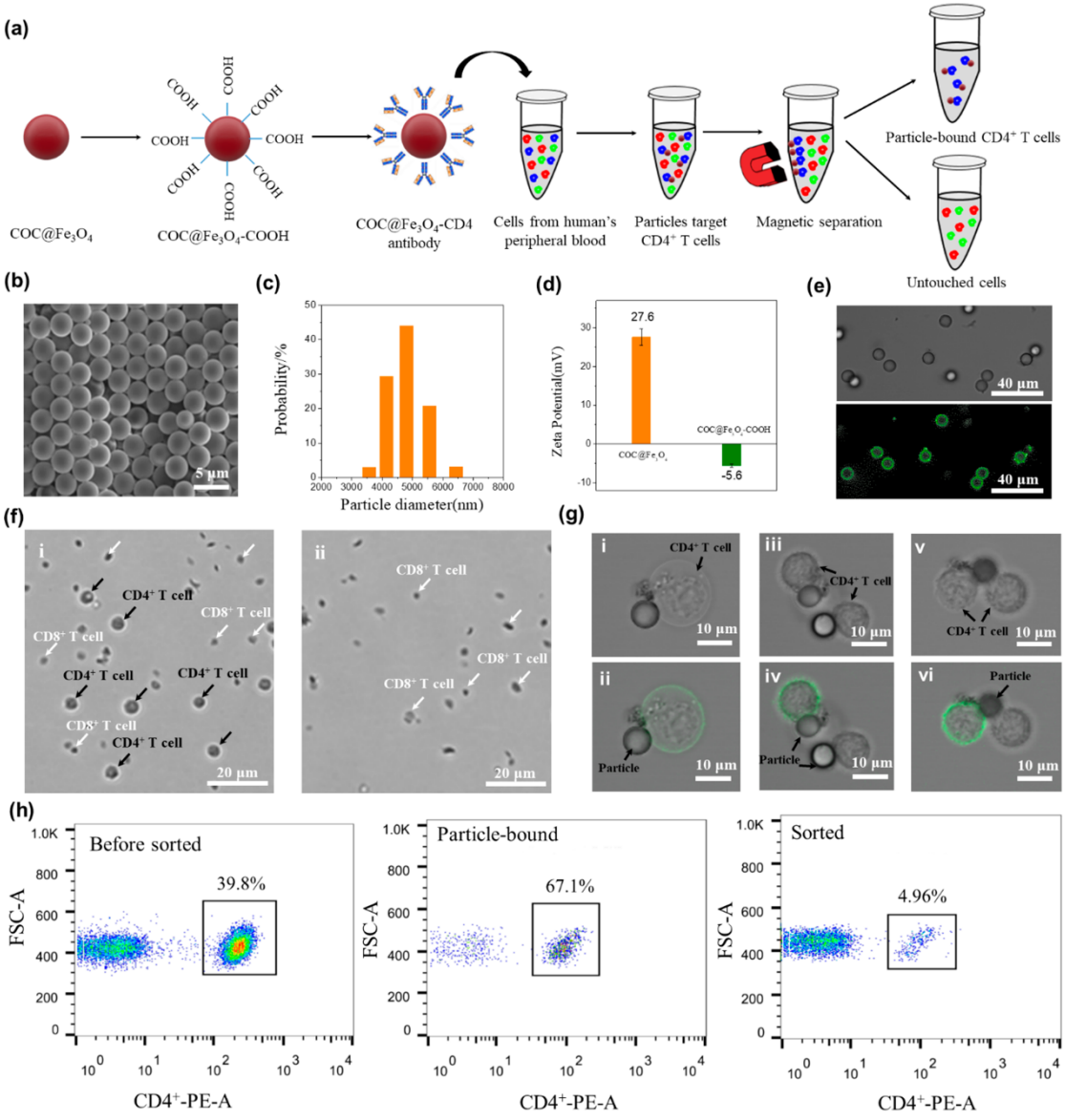

Figure 5. Bioseparation applications. (a) Schematic of the cell-separation process. (b, c) SEM image and size distribution of the particles, respectively. (d) The ζ potential of the particles before and after modification. (e) Bright-field and fluorescent images of the particles coupled with FITC. (f) Fluorescent images of the cells before (i) and after separation (ii). (g) Bright-field and overlay images of the particles bonded to $CD4^+$ T cells after isolation. (h) Statistical results of cell-separation efficiency.

The available magnetic–polymeric particles with fast magnetic response and excellent biological compatibility can be exploited for the development of bioseparation systems. As proof, we demonstrated that these particles can be used for the precise extraction of $CD4^+$ T cells from the blood, which are critical for assessing the human immune system. The experimental principle is based on the specific binding between an antibody and an antigen. As schematically shown in

Figure 5a, carboxyl-modified magnetic−polymeric particles (COC@ Fe_3O_4-COOH) were covalently bonded to a primary CD4 monoclonal antibody through a secondary human antimouse IgG antibody. The particles coupled with the primary CD4 monoclonal antibody were thoroughly mixed with human peripheral blood mononuclear cells (PBMCs). The magnetic− polymeric particles carried with the $CD4^+$ T cells were selectively collected by applying an external magnetic field and were further separated into a release buffer.

Selecting the optimal particle size is the most critical aspect for their application to biological separation. Thus, we systematically analyzed the particles-size-dependent particle− cell interactions by exploiting the advantages of the PRI approach for tuning the particle size. As expected, the targeted magnetic−polymeric particles with a diameter of ∼5 ± 0.1 μm exhibited the best performance, because such large particles easily settle, whereas small ones are highly likely to be endocytosed by the cells.[38,39] The typical SEM image and the size distribution indicated the high uniformity of the used particles (Figures 5b and 5c). The ζ potential measurements showed that the particle surface charge changed from +27.6 mV to −5.6 mV after the surface modification, implying that the carboxyl group successfully anchored on the surface of the COC@Fe_3O_4 particles (Figure 5d).

To examine the binding potential between the COC@ Fe_3O_4-COOH particles and an antibody, the fluorescent antibody fluorescein isothiocyanate (FITC) was used, and the laser confocal fluorescence microscopy verified the existence of a strong coupling between the particles and the antibody (Figure 5e). Then, the CD4 antibody was bonded to the particles, and the biological separation performance was studied (Figure 5f,g). As shown in Figure 5f (i), the PBMCs contained many kinds of cells, such as $CD4^+$ and $CD8^+$ T cells, and the percentage of $CD4^+$ T cells with a spherical shape was estimated to be ∼39.8%. When the PBMCs were brought close to the magnetic−polymeric particles, the quantity of $CD4^+$ T cells sharply decreased, as depicted in the fluorescence optical microscopy image (Figure 5f (ii)). The bright-field and the overlay laser confocal fluorescence microscopy images of the separated magnetic particles distinctly showed two representative coupling cases, namely, one particle−one $CD4^+$ T cell (Figure 5g (i, iii) and (ii, iv)) and one particle−two $CD4^+$ T cells (Figure 5g (v) and (vi)), respectively. Flow cytometry analysis (Figure 5h) calculated the absolute separation efficiency of ∼67.1% for $CD4^+$ T cells. Overall, these results demonstrate that the constructed magnetic−polymeric par- ticles can effectively separate and purify $CD4^+$ T cells. In contrast to the conventional biological separation agent, which strictly relies on polystyrene beads, our magnetic−polymeric particles offer multiple advantages, including excellent protein adsorption ability,[40] outstanding biological compatibility,[41] and superior resistance to chemical acids, alkalis, and most organic polar solvents (e.g., ethyl acetate, acetone, and isopropyl alcohol).[42] Furthermore, our magnetic−polymeric particles can be used to separate not only $CD4^+$ T cells but also other cells, proteins, and nucleic acids.

CONCLUSIONS

We proposed a scalable method for the fabrication of magnetic–polymeric particles with an extremely wide tuna- bility range of ~20 nm to ~1.25 mm in diameter. The fabrication route, which involved the in-fiber fluid dynamical instability, provided a convenient access to various function-alized polymer-derived particles, which were otherwise difficult to obtain by conventional chemical polymerization methods. The successful fabrication of magnetic COC@Fe_3O_4 particles and their application for heavy-metal recovery and $CD4^+$ T cell sorting were demonstrated. Given that the proposed method surpassed the compatibility constraints for structure hybridization, the approach can serve as a universal route for encapsulating various functional building blocks in magnetic– polymeric particles and modulating their combinations. This work is a major step toward the next-generation magnetic particles with luminescent and electrical properties that may outperform conventional magnetic particles.

EXPERIMENTAL SECTION

Preform Fabrication and Fiber Drawing. The core/cladding (COC/PMMA) fiber (Figure 1) was constructed as follows: (i) A cylindrical rod of COC (diameter: 3 mm) was extruded at 240 °C through a circular die in vacuum by using the as-purchased millimeter-sized pellets (Zeon Chemicals, Japan). (ii) The COC rod was inserted into a PMMA tube (Hua Xia Plastic Technology, China) with an inner diameter of 3 mm and outer diameters of 20, 25, 30, 35, and 40 mm. Then, the resultant cylinders were consolidated into preforms at 200 °C for 30 min under vacuum. (iii) The preforms were thermally drawn into fibers with various diameters in a fiber-drawing tower. The procedure for fabricating magnetic–polymeric particles can be summarized as follows: (i) The COC pellets were mixed with Fe_3O_4 nanoparticles (Aladdin, China) by melt compounding. (ii) Then, the melt was extruded into a rod (diameter: 3 mm) at 240 °C through a circular die. (iii) The rod was inserted into a PMMA tube (Hua Xia Plastic Technology, China) with an inner diameter of 3 mm and an outer diameter of 30 mm. Then, the resultant cylinder was consolidated into a preform at 200 °C for 30 min in vacuum. (iv) The preform was thermally drawn into fibers in a fiber-drawing tower. The COC pellets compounded with a fluorescent dye or QDs were fabricated as follows: (i) The COC pellets and the fluorescent dye or QDs were dissolved in chloroform solution (Sigma–Aldrich) and stirred at 70 °C for 24 h. (ii) Then, the chloroform solution was evaporated in a vacuum furnace until the COC was completely dried. (iii) The raw material was extruded into a rod (diameter, 10 mm; length, ~50 cm) at ~190 °C. Then, the rod was used for fiber drawing.

Particles Release. After the fibers were annealed to induce the PRI, the particles were released by dissolving the PMMA cladding in N,N-dimethylacetamide solution (DMAC; Sigma–Aldrich) at room temperature for 30 min. The magnetic–polymeric particles dispersed in DMAC were separated by centrifugation and washed twice with 2- propanol (Sigma–Aldrich) to remove any remaining DMAC. Then, the particles were washed three times with deionized water and dispersed in deionized water for subsequent use.

Surface Modification with Amino Groups. The magnetic polymeric particles dispersed in deionized water were separated by centrifugation at 12,000 rpm and washed twice with an ethanol–water solution. Finally, the particles were dispersed in the ethanol–water solution (80 vol % ethanol). Then, 4 mL of tetraethyl orthosilicate (TEOS; Sigma–Aldrich) and 2 mL of ammonium hydroxide were added to the solution containing 5 mg mL^{-1} of the magnetic– polymeric particles. The newly formulated solution was mixed for 2 h by ultrasonic dispersion and washed twice with an ethanol–water solution. This solution was mixed with 4 mL of 3-aminopropyl triethoxysilane (APTES; Sigma–Aldrich) and 2 mL of ammonium hydroxide, and the mixture was left in an ultrasonic bath for 2 h. Finally, the mixed solution was centrifuged with deionized water, and the amino-modified magnetic–polymeric particles dispersed in deionized water were used.

Adsorption and Recovery of Heavy-Metal Ions (Cd^{2+}, Co^{2+}, Ni^{2+}, and Cu^{2+}). In the experiments, 20 mg of the amino-modified magnetic–polymeric particles were suspended in 20 mL of deionized water containing different concentrations of Cd^{2+}, Co^{2+}, Ni^{2+}, and Cu^{2+} ions from $Cd(NO_3)_2{\cdot}4H_2O$, $Co(NO_3)_2{\cdot}6H_2O$, $Ni(NO_3)_2{\cdot}6H_2O$, and $Cu(NO_3)_2{\cdot}3H_2O$ salts, respectively. The mixture solution was stirred using a shaker at room temperature for 30 min. After adsorption, the supernatants were magnetically separated using a hand-held magnet (NdFeB permanent magnet). Finally, the adsorbed Cd^{2+}, Co^{2+}, Ni^{2+}, and Cu^{2+} ions were released from the particles in 0.1 mol L^{-1} H_2SO_4 solution.

Regeneration of the Amino-Modified Magnetic–Polymeric Particles. The particles were regenerated by washing them with 0.1 mol L^{-1} NaOH solution for 20 min. Then, these particles were fully washed with deionized water. After the regeneration, the amino- modified magnetic–polymeric particles were reused to separate heavy-metal ions.

Surface Modification with Carboxyl Group. The magnetic– polymeric particles dispersed in deionized water were separated by centrifugation and washed twice with an ethanol–water solution and resuspended in the ethanol–water solution. Then, 4 mL of TEOS and 2 mL of ammonium hydroxide were added to the solution. The mixture was kept in an ultrasonic bath for 2 h and then washed twice with the ethanol–water solution. After which, 4 mL of 3- glycidyloxypropyltrimethoxysilane (Sigma–Aldrich) and 2 mL of ammonium hydroxide were added, and the mixture was shocked for 3 h and washed twice with the ethanol–water solution. After that, the mixture was washed twice with methyl alcohol and then dispersed in it. Then, 1 mL of sodium iminodiacetate dibasic monohydrate (Sigma–Aldrich) solution was added, and then the mixture was shocked in a water bath at room temperature for 48 h. The shocked solution was washed twice with methyl alcohol and another two times with HCl solution (pH 3). Finally, the particles were dispersed in deionized water for subsequent use.

Cell-Separation Process. First, we prepared a single-cell suspension of lymphocytes from human PBMCs at the concentration of 1×10^8 cells mL^{-1} in the desired cell-separation buffer with 0.5% bovine serum albumin (BSA; Thermo Fisher). Then, 50 μL of carboxyl-modified magnetic–polymeric particles (5 mg mL^{-1}) was transferred to the tube with a volume of 1.5 mL and was washed twice with phosphate buffer saline (PBS;

Thermo Fisher) solution at pH 7.4. Finally, the particles were resuspended in 0.1 mL of PBS solution at pH 7.4. Next, 20 μL of the CD4 monoclonal antibody (Thermo Fisher), which can target $CD4^+$ T cells, was added to the tube. The mixture was gently shaken for 30 min, and the antibody-bound particles were separated and washed using a magnetic decantation. The antibody-bound particles were resuspended in 0.5 mL of PBS solution at pH 7.4. Then, 100 μL of cell buffer was transferred to the tube, and the mixture was incubated for 10 min under gentle tilting and rotation. Finally, the magnetic−polymeric particles that were bonded to $CD4^+$ T and other cells in the mixture solution were separated by a magnet. The cell-separation efficiency was examined by flow cytometry. The $CD4^+$ T cells can be further released from the surface of magnetic−polymeric particles by adding a releasing buffer, which is composed of a modified biotin in 0.1% BSA and 2 mM EDTA. The release yield was estimated to be larger than 90%.

Material Characterization. The optical images and cross sections of the fibers were captured by a Leica MDI5000 microscope (Germany). The SEM images of particles were obtained using a Merlin SEM (30 kV BSE Zeiss, Germany). The TEM micrographs were measured by using a JEOL-2100F microscope. The size distributions of the particles were measured by DLS (Malvern Zetasizer Nano ZS). The magnetic measurements of the magnetic polymer particles were performed at room temperature in magnetic fields of up to 10 kOe by using a VSM (Mpms XL-7, Quantum Design). The ζ potentials of the synthesized functional particles were measured in deionized water by using a Zeta Sizer (Nano ZS 3600, Nano Series, UK). The concentrations of Cd^{2+}, Co^{2+}, Ni^{2+}, and Cu^{2+} were detected by ICP-AES (Analysis of General Instrument Corporation, China). The images of the cells and particle-bound $CD4^+$ T cells were measured using a confocal laser scanning microscope (Carl Zeiss LSM 710, Jena, Germany) at an excitation wavelength of 488 nm. The cells were measured using the FACSCalibur flow cytometer and the FlowJo software.

ACKNOWLEDGMENTS

The authors gratefully acknowledge financial support from the National Key R&D Program of China (2018YFB1107200), the National Natural Science Foundation of China (Grant 11474102), the National Science Fund for Excellent Young Scholars of China (grant 51622206), the Local Innovative and Research Teams Project of Guangdong Peal River Talents Program (grant 2017BT01X137), the Tip-Top Scientific and Technological Innovative Youth Talents of Guangdong Special Support Program (grant 2015TQ01C362), the Fundamental Research Funds for the Central University, and the Open Fund of State Key Laboratory of Information Photonics and Optical Communications (Beijing University of Posts and Tele- communications), P. R. China (IPOC2016B003).

REFERENCES

(1) Song, G.; Chen, M.; Zhang, Y.; Cui, L.; Qu, H.; Zheng, X.; Wintermark, M.; Liu, Z.; Rao, J. Janus Iron Oxides @ Semiconducting Polymer Nanoparticle Tracer for Cell Tracking by Magnetic Particle Imaging. Nano Lett. 2018, 18, 182−189.

(2) Upadhyay, M.; Adena, S.; Vardhan, H.; Yadav, S.; Mishra, B. Development of Biopolymers Based Interpenetrating Polymeric Network of Capecitabine: A Drug Delivery Vehicle to Extend the Release of the Model Drug. Int. J. Biol. Macromol. 2018, 115, 907–

(3) Goswami, L.; Kim, K.; Deep, A.; Das, P.; Bhattacharya, S.; Kumar, S.; Adelodun, A. Engineered Nano Particles: Nature, Behavior, and Effect on the Environment. J. Environ. Manage. 2017, 196, 297–315.

(4) Yu, X.; Liu, H.; Diao, J.; Sun, Y.; Wang, Y. Magnetic Molecularly Imprinted Polymer Nanoparticles for Separating Aromatic Amines from Azo Dyes-Synthesis, Characterization and Application. Sep. Purif. Technol. 2018, 204, 213–219.

(5) Wang, M.; Yin, Y. Magnetically Responsive Nanostructures with Tunable Optical Properties. J. Am. Chem. Soc. 2016, 138, 6315–6323.

(6) Huang, L.; Bai, G.; Wong, M.; Yang, Z.; Xu, W.; Hao, J. Magnetic-Assisted Noncontact Triboelectric Nanogenerator Convert- ing Mechanical Energy into Electricity and Light Emissions. Adv. Mater. 2016, 28, 2744–2751.

(7) Wong, M.; Chen, L.; Tsang, M.; Zhang, Y.; Hao, J. Magnetic- Induced Luminescence from Flexible Composite Laminates by Coupling Magnetic Field to Piezophotonic Effect. Adv. Mater. 2015, 27, 4488–4495.

(8) Bai, M.; Moran, C.; Zhang, L.; Liu, C.; Zhang, Y.; Wang, L.; Xia, Y. A Facile and General Method for the Encapsulation of Different Types of Imaging Contrast Agents within Micrometer-Sized Polymer Beads. Adv. Funct. Mater. 2012, 22, 764–770.

(9) Kawaguchi, H. Functional Polymer Microspheres. Prog. Polym. Sci. 2000, 25, 1171–1210.

(10) Cao, G.; Wang, Y. Nanostructures and Nanomaterials: Synthesis, Properties and Applications; Imperial College Press: London, 2004; pp 1–20.

(11) Merkel, T.; Herlihy, K.; Nunes, J.; Orgel, R.; Rolland, J.; DeSimone, J. Scalable, Shape-Specific, Top-Down Fabrication Methods for the Synthesis of Engineered Colloidal Particles. Langmuir 2010, 26, 13086–13096.

(12) Sanchez, L.; Martin, D.; Alvarez, V.; Gonzalez, J. Polyacrylic Acid-Coated Iron Oxide Magnetic Nanoparticles: The Polymer Molecular Weight Influence. Colloids Surf., A 2018, 543, 28–37.

(13) Utada, A.; Lorenceau, E.; Link, D.; Kaplan, P.; Stone, H.; Weitz, D. Monodisperse Double Emulsions Generated from a Microcapillary Device. Science 2005, 308, 537–541.

(14) Dendukuri, D.; Doyle, P. The Synthesis and Assembly of Polymeric Microparticles Using Microfluidics. Adv. Mater. 2009, 21, 4071–4086.

(15) Dendukuri, D.; Pregibon, D.; Collins, J.; Hatton, T.; Doyle, P. Continuous-Flow Lithography for High-Throughput Microparticle Synthesis. Nat. Mater. 2006, 5, 365.

(16) Kelly, J.; DeSimone, J. Shape-Specific, Monodisperse Nano- Molding of Protein Particles. J. Am. Chem. Soc. 2008, 130, 5438– 5439.

(17) Rolland, J.; Maynor, B.; Euliss, L.; Exner, A.; Denison, G.; DeSimone, J. Direct Fabrication and Harvesting of Monodisperse, Shape-Specific Nanobiomaterials. J. Am. Chem. Soc. 2005, 127, 10096–10100.

(18) Serrano García, R.; Stafford, S.; Gun'ko, Y. Recent Progress in Synthesis and Functionalization of Multimodal Fluorescent-Magnetic Nanoparticles for Biological Applications. Appl. Sci. 2018, 8, 172.

(19) Bang, J.; Suslick, K. Applications of Ultrasound to the Synthesis of Nanostructured Materials. Adv. Mater. 2010, 22, 1039–1059.

(20) Lu, A.; Salabas, E.; Schüth, F. Magnetic Nanoparticles: Synthesis, Protection, Functionalization, and Application. Angew. Chem., Int. Ed. 2007, 46, 1222–1244.

(21) Tao, G.; Kaufman, J.; Shabahang, S.; Naraghi, R.; Sukhov, S.; Joannopoulos, J.; Fink, Y.; Dogariu, A.; Abouraddy, A. Digital Design of Multimaterial Photonic Particles. Proc. Natl. Acad. Sci. U. S. A. 2016, 113, 6839–6844.

(22) Kaufman, J.; Ottman, R.; Tao, G.; Shabahang, S.; Banaei, E.; Liang, X.; Johnson, S.; Fink, Y.; Chakrabarti, R.; Abouraddy, A. F. In- Fiber Production of Polymeric Particles for Biosensing and Encapsulation. Proc. Natl. Acad. Sci. U. S. A. 2013, 110, 15549–15554.

(23)Plateau,J.StatiqueExpeŕimentaleetTheóriquedesLiquides SoumisauxSeulesForcesMolećulaires.Acad.Sci.Brux.Mem.1849, 23, 5.

(24) Rayleigh, L. On the Instability of a Cylinder of Viscous Liquid Under Capillary Force. Philos. Mag. 1892, 34, 145–154.

(25) Young, T. An Essay on the Cohesion of Fluids. Philos. Trans. R. Soc. London 1805, 95, 65–87.

(26) Laplace, P. Traite de Mechanique Celeste; Gauthier-Villars: Paris, 1805; Vol. 4.

(27) Kinoshita, C.; Teng, H.; Masutani, S. A Study of the Instability of Liquid Jets and Comparison with Tomotika's Analysis. Int. J. Multiphase Flow 1994, 20, 523–533.

(28) Tomotika, S. On the Instability of a Cylindrical Thread of a Viscous Liquid Surrounded by Another Viscous Fluid. Proc. R. Soc. London, Ser. A 1935, 150, 322–337.

(29) Da Silva, L. W.; Kaviany, M. Micro-Thermoelectric Cooler: Interfacial Effects on Thermal and Electrical Transport. Int. J. Heat Mass Transfer 2004, 47, 2417–2435.

(30) Lamonte, R.; McNally, D. Uses and Processing of Cyclic Olefin Copolymers. Plast. Eng. 2000, 56, 51–56.

(31) Khanarian, G. Optical Properties of Cyclic Olefin Copolymers. Opt. Eng. 2001, 40, 1024–1030.

(32) Monier, M.; Ayad, D.; Wei, Y.; Sarhan, A. Adsorption of Cu (II), Co (II), and Ni (II) Ions by Modified Magnetic Chitosan Chelating Resin. J. Hazard. Mater. 2010, 177, 962–970.

(33) Swayampakula, K.; Boddu, V.; Nadavala, S.; Abburi, K. Competitive Adsorption of Cu (II), Co (II) and Ni (II) From Their Binary and Tertiary Aqueous Solutions Using Chitosan-Coated Perlite Beads as Biosorbent. J. Hazard. Mater. 2009, 170, 680–689.

(34) Smith, S. A. Critical Review of the Bioavailability and Impacts of Heavy Metals in Municipal Solid Waste Composts Compared to Sewage Sludge. Environ. Int. 2009, 35, 142–156.

(35) Srivastava, N.; Majumder, C. Novel Biofiltration Methods for the Treatment of Heavy Metals from Industrial Wastewater. J. Hazard. Mater. 2008, 151, 1–8.

(36) Sud, D.; Mahajan, G.; Kaur, M. Agricultural Waste Material as Potential Adsorbent for Sequestering Heavy Metal Ions from Aqueous Solutions-A Review. Bioresour. Technol. 2008, 99, 6017–6027.

(37) Drinking Water Contaminants, United States Environmental Protection Agency (U.S. EPA), http://water.epa.gov/drink/ contaminants/index.cfm, accessed 30 November 2011.

(38) Wu, W.; Wu, Z.; Yu, T.; Jiang, C.; Kim, W. Recent Progress on Magnetic Iron Oxide Nanoparticles: Synthesis, Surface Functional Strategies and Biomedical Applications. Sci. Technol. Adv. Mater. 2015, 16, 023501.

(39) Safarik, I.; Stepanek, M.; Uchman, M.; Slouf, M.; Baldikova, E.; Nydlova, L.; Pospiskova, K.; Safarikova, M. Composite Particles Formed by Complexation of Poly (methacrylic acid)-Stabilized Magnetic Fluid with Chitosan: Magnetic Material for Bioapplications. Mater. Sci. Eng., C 2016, 67, 486–492.

(40) Kai, J.; Sohn, Y.; Ahn, C. Proceedings of the μTAS 2002 Symposium, Nara, Japan, November 3–7, 2002; Springer Scienc +Business Media, B.V.: Dordrecht, The Netherlands, 2002.

(41) Rohr, T.; Ogletree, D.; Svec, F.; Freć het, J. Surface Functionalization of Thermoplastic Polymers for the Fabrication of Microfluidic Devices by Photoinitiated Grafting. Adv. Funct. Mater. 2003, 13, 264–270.

(42) Jena, R.; Yue, C. Cyclic Olefin Copolymer Based Microfluidic Devices for Biochip Applications: Ultraviolet Surface Grafting Using 2-methacryloyloxyethyl Phosphorylcholine. Biomicrofluidics 2012, 6, 012822.